JOURNAL OF GEOPHYSICAL RESEARCH, VOL. 108, NO. D8, 4233, doi:10.1029/2002JD002560, 2003

Global modeling of the isotopic analogues of N_2O: Stratospheric distributions, budgets, and the ^{17}O–^{18}O mass-independent anomaly

Chris A. McLinden
Meteorological Service of Canada, Downsview, Ontario, Canada

Michael J. Prather
Department of Earth System Science, University of California at Irvine, Irvine, California, USA

Matthew S. Johnson
Department of Chemistry, University of Copenhagen, Copenhagen, Denmark

Received 23 May 2002; revised 21 November 2002; accepted 14 January 2003; published 17 April 2003.

[1] A three-dimensional chemical transport model (CTM) is used to study the stratospheric distributions and global budgets of the five most abundant isotopic analogues of N_2O: $^{14}N^{14}N^{16}O$, $^{14}N^{15}N^{16}O$, $^{15}N^{14}N^{16}O$, $^{14}N^{14}N^{18}O$, and $^{14}N^{14}N^{17}O$. Two different chemistry models are used to derive photolysis cross sections for the analogues of N_2O: (1) the zero-point energy shift model, scaled by a factor of 2 to give better agreement with recent laboratory measurements and (2) the time-dependent Hermite propagator model. Overall, the CTM predicts stratospheric enrichments that are in good agreement with most measurements, with the latter model performing slightly better. Combining the CTM-calculated stratospheric losses for each N_2O species with current estimates of tropospheric N_2O sources defines a budget of flux-weighted enrichment factors for each. These N_2O budgets are not in balance, and trends of -0.04 to -0.06 ‰/yr for the mean of $^{14}N^{15}N^{16}O$ and $^{15}N^{14}N^{16}O$ and -0.01 to -0.02 ‰/yr for $^{14}N^{14}N^{18}O$ are predicted, although each has large uncertainties associated with the sources. The CTM also predicts that $^{14}N^{14}N^{17}O$ and $^{14}N^{14}N^{18}O$ will be fractionated by photolysis in a manner that produces a nonzero mass-independent anomaly. This effect can account for up to half of the observed anomaly in the stratosphere without invoking chemical sources. In addition, a simple one-dimensional model is used to investigate a number of chemical scenarios for the mass-independent composition of stratospheric N_2O. *INDEX TERMS:* 0317 Atmospheric Composition and Structure: Chemical kinetic and photochemical properties; 0322 Atmospheric Composition and Structure: Constituent sources and sinks; 0341 Atmospheric Composition and Structure: Middle atmosphere—constituent transport and chemistry (3334); 1040 Geochemistry: Isotopic composition/chemistry; 3337 Meteorology and Atmospheric Dynamics: Numerical modeling and data assimilation; *KEYWORDS:* global model, N_2O, isotopomer, isotopologue, stratosphere, fractionation

Citation: McLinden, C. A., M. J. Prather, and M. S. Johnson, Global modeling of the isotopic analogues of N_2O: Stratospheric distributions, budgets, and the ^{17}O–^{18}O mass-independent anomaly, *J. Geophys. Res.*, *108*(D8), 4233, doi:10.1029/2002JD002560, 2003.

1. Introduction

[2] Nitrous oxide (N_2O) plays two key roles in the Earth's atmosphere: it is a chemically active gas [*Bates and Hays*, 1967; *Crutzen*, 1970; *McElroy and McConnell*, 1971], the primary source of stratospheric nitrogen oxides involved in catalytic ozone loss; and it is an important greenhouse gas [*Yung et al.*, 1976; *Ramanathan et al.*, 1985]. Its atmospheric abundance has been increasing since the nineteenth century [*Battle et al.*, 1996; *Flückiger et al.*, 1999], indicating a 50% increase in sources that is associated with human activities.

[3] Sources of atmospheric N_2O are predominantly from surface or near-surface emissions. The only known sink of atmospheric N_2O is chemical loss in the stratosphere. Based on a combination of measurements and models, stratospheric loss of N_2O is reasonably well quantified in recent evaluations [e.g., *Park et al.*, 1999; *Prinn and Zander*, 1999; *Prather and Ehhalt*, 2001] at about 13 Tg(N)/yr to within ±20%. Photolysis (between 185–220 nm) comprises about 90% of the loss while reaction with $O(^1D)$ accounts for the rest.

$$N_2O + h\nu \xrightarrow{J} N_2 + O \tag{1a}$$

$$N_2O + O(^1D) \xrightarrow{k} N_2 + O_2 \text{ or } 2NO \tag{1b}$$

0148-0227/03/2002JD002560

J and k represent the photolysis rate coefficient (J-value) and kinetic reaction rate coefficient (sum of both channels), respectively. The second $O(^1D)$ channel represents the predominant source of reactive nitrogen (NO_x) in the stratosphere.

[4] The sources of atmospheric N_2O are multitude with both anthropogenic and natural components. Primarily, they involve biological nitrogen cycling in the land and ocean reservoirs, and secondarily they result from chemical conversion of nitrogen compounds (e.g., combustion, atmospheric oxidation of NH_3). The source strengths based on emissions inventories, however, remain elusive, and hence also do strategies to reduce anthropogenic emissions. Source strengths from different inventories vary widely, with most individual components known only to a factor of 2 to 4. For example, the largest single anthropogenic source is agricultural soils, which is estimated to be 4.2 Tg(N)/yr but with a range of 0.6 to 14.8 Tg(N)/yr. Even the total source strength from emissions inventories has a range of at least ±50% [*Mosier et al.*, 1998; *Olivier et al.*, 1998; *Kroeze et al.*, 1999; *Prather and Ehhalt*, 2001]. The best constraint on the current source strength is based on the observed annual increase in surface abundance [*Weiss*, 1981; *Prinn et al.*, 2000]: i.e., the total source strength currently exceeds the sink by about 4 Tg(N)/yr with an uncertainty of only ±10%.

[5] Analysis of stable isotopes is a promising means of constraining N_2O sources as the different components possess varied isotopic signatures [e.g., *Kim and Craig*, 1990; *Pérez et al.*, 2000, 2001]. This approach has great potential because there are four isotopically substituted species abundant enough to measure. In addition to the primary species $^{14}N^{14}N^{16}O$ (or 446 for short where each digit in '446' refers to the second digit in the mass number of the N, N, and O atoms), there are four isotopic analogues which possess one rare nuclide. These consist of two oxygen isotopologues that differ by simple isotopic substitution ($^{14}N^{14}N^{17}O$ (447) and $^{14}N^{14}N^{18}O$ (448)), and two isotopomers of the nitrogen isotopologue that differ by the position of the substitution ($^{14}N^{15}N^{16}O$ (456) and $^{15}N^{14}N^{16}O$ (546)). Molecules with two or three rare nuclides are orders of magnitude less abundant and not considered in this study. Nevertheless, the isotopic constraints on the budget suffer from a lack of information regarding the isotopic composition of the N_2O sources, and the enrichment of the heavy nuclides by photolysis and possible in situ chemistry.

[6] Measurements have been carried out for the largest source components, but the isotopic composition of individual sources generally possess large uncertainties [e.g., *Rahn and Wahlen*, 2000] and there are possible systematic biases between labs in the definition of the zero of the scale. Furthermore, these spatially and temporally sparse measurements must be generalized for global, annual budget assessments. For some of the smaller sources, no measurements of their isotopic signatures have been made. Adding to this problem is uncertainty regarding the role of the stratospheric sink. This study focuses on refining the stratospheric budget for the isotopic analogues of N_2O and thus eliminating a major uncertainty in these budgets.

[7] Recent measurements indicate that stratospheric N_2O is enriched in rare N and O nuclides relative to the troposphere but reports differ as to the size of this effect [e.g., *Rahn and Wahlen*, 1997; *Griffith et al.*, 2000; *Toyoda et al.*, 2001]. It was originally reported that photolysis did not lead to an appreciable enrichment of the rare nuclides [*Johnston et al.*, 1995] yet more recent experiments indicate a substantial enrichment [e.g., *Rahn et al.*, 1998; *Röckmann et al.*, 2000]. Predictions from a theoretical model of photolysis enrichment, called the zero-point energy (ZPE) shift model [*Yung and Miller*, 1997], agree qualitatively with these most recent experiments but not quantitatively. The time-dependent Hermite propagator (HP) model [*Johnson et al.*, 2001] offers better agreement with the laboratory measurements. These theoretical models are needed to extend the limited laboratory measurements to a full range of wavelengths, isotopic analogues, and temperatures. One additional source of confusion over the past half-decade has been in understanding the origin of an anomaly observed in the abundance of 447 relative to that of 448 - a so-called mass-independent anomaly [e.g., *Cliff and Thiemens*, 1997].

[8] A large number of recent studies have reported measurements of (i) the relative isotopomer and isotopologue distribution in sources, (ii) the tropospheric and stratospheric species distributions, and (iii) the photolytic enrichment factors measured in the lab. The present work fills substantial gaps in our knowledge and allows us to try to close the N_2O nuclide budgets with state-of-the-art modeling of the enrichments occurring during stratospheric loss. We simulate the individual N_2O species in a three-dimensional atmospheric chemical transport model (CTM) that has been calibrated for stratospheric tracers and the rate of stratosphere-troposphere exchange [*McLinden et al.*, 2000; *Avallone and Prather*, 1997]. Section 2 describes both chemistry and transport models, and section 3 presents the stratospheric distributions. These simulations are tested with atmospheric observations and allow us to derive with high confidence the tropospheric composition due to the stratospheric sink. The (456 + 546)/2 and 448 N_2O budgets are given in section 4. Possible origins of the mass-independent oxygen anomaly are presented in section 5; and the conclusions, in section 6.

2. Modeling of Isotopic Analogues in the UCI CTM

[9] The isotopic composition is characterized by the 'delta value', δ. This variable denotes the abundance of one of the rare isotopomers (X) relative to that of 446 with respect to some standard:

$$\delta^X = \frac{R^X}{R_0^X} - 1 \tag{2}$$

where $R^X = [X]/[446]$ is the heavy-to-light isotope ratio of species X, where X = 546, 456, 447, 448, or (546 + 456)/2 and R_0^X refers to the isotope ratio of the standard. Delta values are usually expressed as a 'per mil' quantity (or '‰' where 1‰ = 0.1%) and so would be multiplied by a factor of 1000. In this case the R_0^X refers to the ratio $^{15}N/^{14}N$, $^{17}O/^{16}O$, or $^{18}O/^{16}O$ in air (that is, atmospheric N_2 and O_2). For much of this evaluation we focus on the composition relative to the bulk tropospheric abundance and define δ* so that mean tropospheric N_2O has δ* = 0. That is,

$$\delta^{*X} = \delta^X - \delta^X(\text{tropospheric } N_2O) \tag{3}$$

The δ^X of tropospheric N_2O is taken as +7‰ for the ^{15}N (=(456 + 546)/2) isotopomers and +19‰ for the ^{18}O (=448) isotopologues [*Cliff and Thiemens*, 1997; *Yoshida and Toyoda*, 2000].

[10] The fractionation resulting from a given process is characterized by the enrichment factor, ϵ. In this paper we generally use ϵ in concert with an additional symbol to identify a specific type of enrichment factor. For example, ϵL^X is defined as the enrichment factor for chemical loss of species X relative to 446 in the stratosphere (also defined below). In addition, as a result of a fractionating process isotopic compositions are shifted. If the enrichment factor is constant and relatively small (say $|\epsilon| < 25$‰) then the isotopic composition is related to the fraction of 446 remaining, f, by $\delta^X = \delta_0^X + \epsilon^X \ln f$, where δ_0^X represents the initial composition of species X. This is called a Rayleigh distillation. To be consistent with other recent publications, when referring to an enrichment factor for such a distillation process we simply use the symbol ϵ^X.

[11] The University of California at Irvine (UCI) chemistry-transport model (CTM) [*McLinden et al.*, 2000; *Wild and Prather*, 2000; *Olsen et al.*, 2001] is used to simulate the five N_2O species distributions. The CTM has sufficiently accurate numerics and low numerical noise such that each isotopomer and isotopologue can be modeled as an independent species to a relative precision of better than 0.1‰. Chemical loss of the primary species, 446, is implemented using loss frequencies (J + k[O(^1D)] from reaction 1) that are pre-calculated in a photochemical box model as a function of latitude, altitude, and time of year using standard atmospheres and chemical rate data and cross sections [*Hall and Prather*, 1995; *Sander et al.*, 2000]. The rare N_2O species have cross section and rate coefficients that differ slightly from 446, typically by 1–2%, and it is this small difference which gives rise to their fractionation relative to 446.

[12] For photolytic loss, we employ two chemistry models. The zero-point energy shift model of *Yung and Miller* [1997; *Miller and Yung*, 2000] estimates the shift in photolysis cross sections based on the change in the frequencies of the fundamental vibrational modes associated with the additional mass of the rare nuclides. The zero-point energy is the amount of energy in a molecule at zero degrees Kelvin, specifically, one half of a quantum in each vibrational mode. For each isotopomer, the shift is equivalent to a blue shift of the 446 cross sections by 0.1–0.2 nm. As discussed below, a factor of 2 increase in the shift is needed to reach agreement with the laboratory data, and we adopt this doubled zero-point energy shift model (hereafter referred to as the ZPE2 model) for use in our CTM simulations. The HP model of *Johnson et al.* [2001] predicts relative cross sections using a first-principles model that includes the transition dipole surface, bending vibrational excitation, dynamics on the excited state potential surface, and factors related to isotopic substitution itself. For both models the cross sections of the rare species are less than those of 446 between 183 and 225 nm, the spectral window in which atmospheric loss of N_2O occurs, and lead to a reduction in the substituted species' J-value relative to 446. The reduction in cross section is not uniform with wavelength; and, since the photolysis occurs at different wavelengths at different altitudes throughout the stratosphere, the relative reduction in J-values is altitude dependent.

[13] The photolytic enrichment factors from recent laboratory experiments [*Rahn et al.*, 1998; *Umemoto*, 1999; *Röckmann et al.*, 2000, 2001b; *Turatti et al.*, 2000; *Zhang et al.*, 2000] are compared with the ZPE2 and HP models in Figure 1. Relative photolytic enrichment factors for the rare species are defined as,

$$\epsilon\sigma^X = \frac{\sigma^X(\lambda)}{\sigma^{446}(\lambda)} - 1 \tag{4}$$

where σ denotes absorption cross section. We assume an equal mix of 456 and 546 when experimental techniques are unable to distinguish them. Negative enrichment factors arise when the photolysis rate of the rare species is smaller than that of 446, and so these species will become relatively more abundant in the stratosphere than in the troposphere (i.e., $\delta^* > 0$).

[14] The original zero-point energy shift model as well as the adopted ZPE2 model are shown in Figure 1. The reason for the underestimate by the original zero-point energy model is likely related to this model's implicit assumptions [e.g., *Zhang et al.*, 2000; *Johnson et al.*, 2001; *Yung and Miller*, 1997], including the assumption that the excited state is purely repulsive and that the transition dipole does not change with the internuclear coordinates. We adopt this revised model, ZPE2, for the remainder of this study. The HP model predicts the cross sections of isotopomers and isotopologues in specific bending vibrational quantum states from first principles, using a two-dimensional potential energy surface (PES) and transition dipole surface, the two dimensions being NN to O distance and bending angle [*Brown et al.*, 1999]. The cross section of a given isotopic analogue at a given temperature is determined using the relative population of each bending vibrational state. Thus the model provides temperature dependent cross sections. The model is in agreement with available experimental data to within the estimated error, 10‰. The largest discrepancy (ca. 10‰) is seen for the 546 isotopomer. The reason why specifically this isotopologue may be more sensitive to the two dimensional approximation than the others has to do with the distribution of mass within the molecule. For an impulse between NN and O, dissociation of 546 will give rise to more NN vibrational excitation within NNO* than 456. However because the best available PES does not take NN motion into account, this leads to a larger error via the 2D PES approximation for the 546 isotopomer. We intend to recalculate the isotopologue and isotopomer cross sections using the three dimensional PES when it becomes available.

[15] Loss of N_2O through the reaction with O(^1D) uses reaction rate coefficients for 446 [*Sander et al.*, 2000] modified by a prescribed enrichment factor: −6‰ for 448 and −3‰ for 447, based on laboratory measurements [*Johnston et al.*, 1995] (i.e., $k^{448} = 0.994k^{446}$). No laboratory studies are available for the 546 and 456 isotopomers, and so a value of −6‰ is assumed for each. As this loss channel represents only 10% of the total, errors here will not significantly impact the overall stratospheric distribution. In the lower stratosphere loss via O(^1D) can be comparable with photolysis but the overall loss rate in this region is lower by a factor of ∼50 compared to the middle stratosphere.

[16] The primary source of meteorological fields for these CTM simulations is the GISS II general circulation model

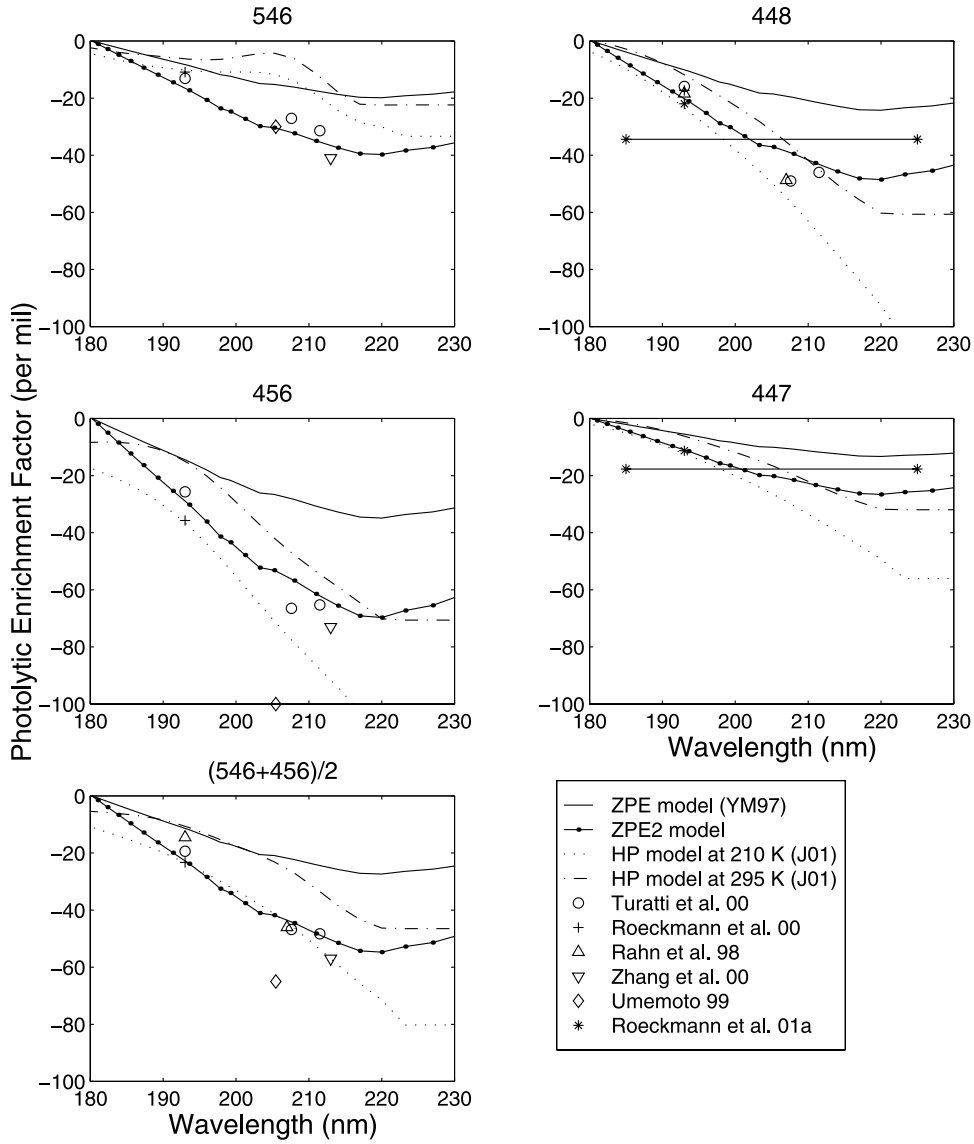

Figure 1. Comparison of laboratory measurements of N_2O isotopic analogue photolytic enrichment factors (in ‰) with predictions from the zero-point energy shift model [*Yung and Miller*, 1997] (YM97), 2× the zero-point energy shift model, and the time-dependent Hermite propagator model [*Johnson et al.*, 2001] (J01) at two temperatures: 210 and 295 K. The *Röckmann et al.* [2001a] data points are derived from isotopic analogue J-value experiments; their data shown connected with the horizontal line are broadband results and represent an integrated photolytic enrichment factor over that wavelength range.

(GCM) [*Rind et al.*, 1988] run at a resolution of 7.8° latitude × 10° longitude × 23 layers with the top three GCM layers combined into one CTM layer. Results from a second simulation are also shown using meteorology GISS II′ GCM [*Koch and Rind*, 1998] run at a resolution of 4° latitude × 5° longitude × 31 layers but degraded to 8° latitude × 10° longitude with the top 9 GCM layers combined into one CTM layer. This latter model is known to have a somewhat stagnant upwelling in the tropical middle stratosphere which leads to unrealistically long N_2O lifetimes, and this has been traced to GCM numerics [*Olsen et al.*, 2001; *Rind et al.*, 2001]. Comparison of the simulations with the different GISS meteorological fields, with quite different N_2O lifetimes, gives an indication of the sensitivity of the stratospheric delta values to model circulation. In the CTM simulations, each of the isotopic species is run to an annually repeating steady-state using an arbitrary lower boundary condition of 310 ppb, and thus the isotopic composition relative to the mean tropospheric abundance (δ^{*X}) is easily calculated from its abundance relative to that of 446. In comparing with observations, we need to shift these delta values by the offset of tropospheric N_2O relative to the laboratory standards: $\delta^{15}N = \delta^{*15}N + 7‰$ and $\delta^{18}O = \delta^{*18}O + 19‰$ [*Cliff and Thiemens*, 1997; *Yoshida and Toyoda*, 2000].

[17] Modeling each isotopically distinct species as a separate tracer (as opposed to transporting the composition

as a rational number) is inherently more straightforward but requires numerical precision of better than 1 part in 10^4, or 0.1‰. This is exceedingly difficult for any tracer transport scheme since, even within the same CTM, changes in flux limiters or the order of polynomial fitting can change results near tracer gradients by several percent or more. We test this within the UCI CTM by altering the limits on the second-order moments of the tracer distribution within each grid box from (method 1) the original positive-definite limiter to (method 2) the current positive-definite-monotonic limiter. Figure 2 shows δ^{448} as a function of ln f for these two simulations. The solid line is a distillation curve calculated by e-folding both 446 and 448 based on their relative stratospheric lifetimes (i.e., mean photolysis frequencies) and then calculating the delta value. The actual isotopologue abundances (symbols) clearly show that the stratosphere, through transport and mixing across different chemical regimes, does not behave as a simple Rayleigh distillation process. Thus, the Rayleigh distillation curve, which can represent the evolution of closed boxes, cannot represent the real world when zero-air (that is, $\delta^* = 0$) is often transported and mixed with partially distilled air. Examining the points as sampled from individual grid boxes, it is clear that the delta values shift slightly between the two limiters, especially in the upper stratosphere (i.e., large values of $-\ln f$). Nevertheless the isotope delta values do not generally differ by more than 0.1‰, particularly in the lower-mid stratosphere where the bulk of the N_2O resides. Figure 2 demonstrates the solid numerics of the CTM in that all model points fall below the e-fold envelope and both numerical limiters generate similar envelopes of delta values.

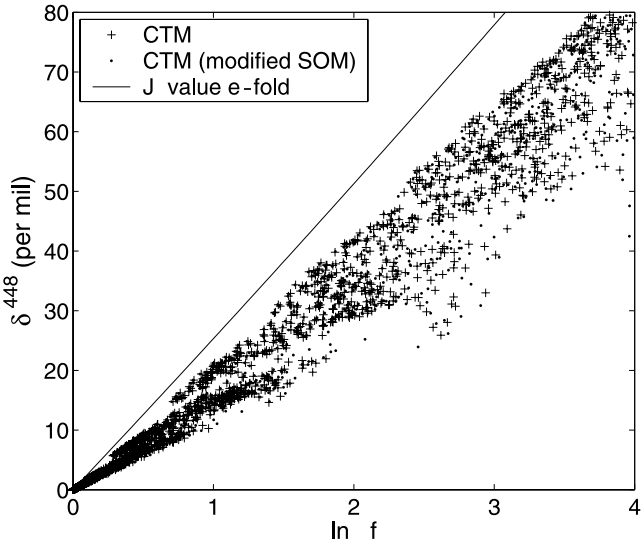

Figure 2. Delta values (using the ZPE2 model) for 448 as a function of $-\ln f$. Shown for the GISS II CTM using standard positive-definite second-order moments (SOM) limiter (+), modified monotonic SOM limiter (·), and J-value e-fold curve (solid line).

3. Stratospheric Fractionation of the N_2O Isotopic Analogues

[18] Steady-state results from the GISS II simulation are presented in Figure 3 for the ZPE2 model and in Figure 4 for the HP model. Shown are the annual, zonal mean 446 mixing ratios (in ppb) and the rare isotopomer and isotopologue delta values (δ^*) plus the average (456 + 546)/2. The delta value is seen to increase rapidly with decreasing N_2O through the stratosphere and the shape of the contours generally mimics that of the 446 mixing ratio. The relative order of enrichments for the ZPE2 model ($\delta^{*456} > \delta^{*448} > \delta^{*546} > \delta^{*447}$) is consistent with measurements [*Rahn and Wahlen*, 1997; *Cliff et al.*, 1999; *Yoshida and Toyoda*, 2000; *Toyoda et al.*, 2001]. The magnitudes in Figure 3 would be a factor of 2 smaller had the predicted wavelength shifts not been doubled (and would clearly disagree with measurements). The HP model enrichments for δ^{*456}, δ^{*447}, and δ^{*448} are almost the same as those for the ZPE2 model, but the HP δ^{*546} is much smaller and is likely an error in the HP 546 model as discussed above.

[19] A summary of the steady-state lifetimes and enrichments due to the stratospheric loss (L in Tg-N/yr) are given in Table 1 for the GISS II meteorology. The annual, global stratospheric loss, related inversely to the global lifetime of 446, are in good agreement with current best estimates [e.g., *Park et al.*, 1999; *Prinn and Zander*, 1999]. The slower loss rates (longer lifetimes) of the rare isotopic analogues are reflected in their lifetimes - as much as 2 years longer than that of 446. The enrichment factors from this stratospheric loss can be calculated from the per mil difference in the loss for each isotopomer,

$$\epsilon L^X = \frac{L^X}{L^{446}} - 1 \tag{5}$$

weighted by the total stratospheric loss of 13.1 Tg(N)/yr for 446. Also presented in Table 1 are the ZPE2 model enrichment factors obtained using the GISS II′ meteorology. The GISS II′ enrichment factors are roughly 16% smaller for all species due likely to the more diffusive nature of its transport. The GISS II model generally has a more advective flow in the sense of the classical residual circulation of the stratosphere [*Andrews and McIntyre*, 1978; *Dunkerton*, 1978] that maintains greater fractionation of the N_2O depleted air re-entering the troposphere.

[20] Specific comparisons between measured and modeled enrichment factors in the stratosphere are presented in Table 2. The measurements are either whole air samples from an aircraft [*Rahn and Wahlen*, 1997], whole air samples from a balloon [*Yoshida and Toyoda*, 2000; *Toyoda et al.*, 2001; *Röckmann et al.*, 2001b], or obtained remotely via occultation from a balloon-borne instrument [*Griffith et al.*, 2000]. For both model and measurements, an enrichment factor for species X (ϵ^X) is calculated from an ensemble of points as the slope of the composition (δ^{*X}) with respect to the natural log of the 446 abundance (relative its tropospheric abundance). The model enrichment factors are obtained by fitting to the following version of the Rayleigh distillation equation, allowing for the offset from the bulk troposphere:

$$\delta^{*X} = \text{constant} + \epsilon^X \ln f \tag{6}$$

In the case of a Rayleigh distillation process over a small range of delta values (not the case for the stratosphere!), this enrichment factor is just the per mil change in the mean lifetime of X relative to that of 446 [e.g., *Griffith et al.*,

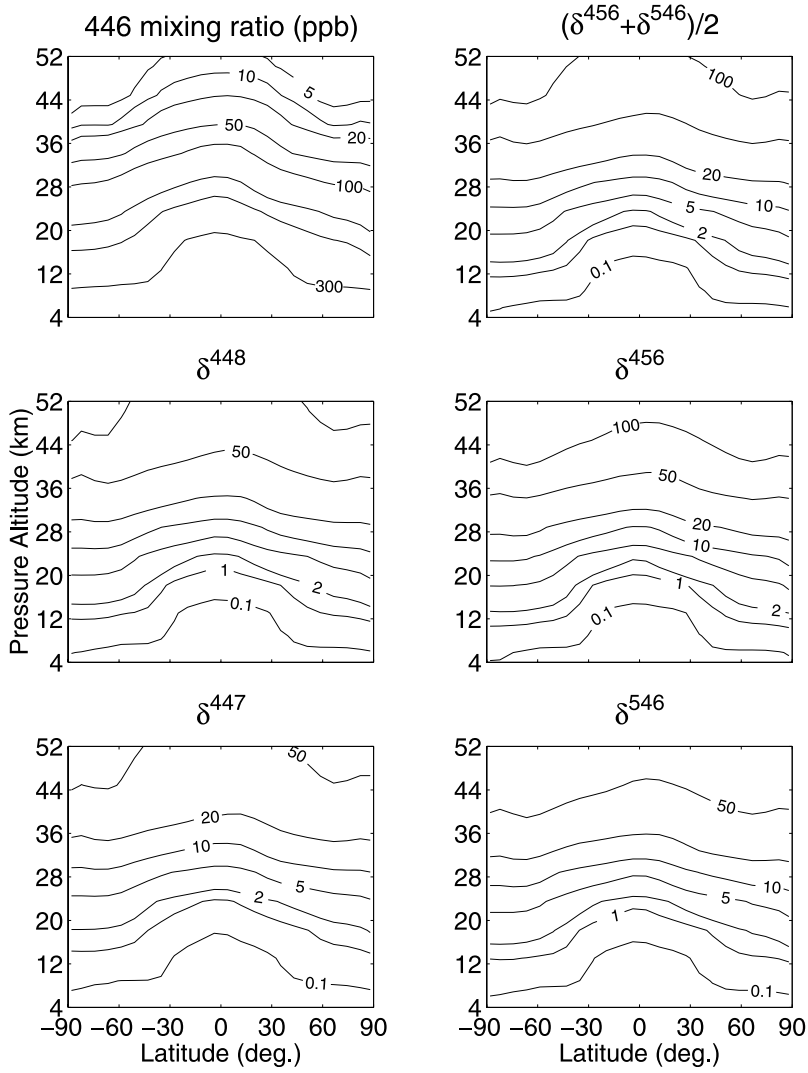

Figure 3. Zonal, annual mean ZPE2 446 abundance (in ppb) and delta values of 456, 546, 448, 447, and (456 + 546)/2 (in ‰). An effective lower boundary condition of $\delta = 0$ was used so these represent the shift in δ from the bulk troposphere. Contour levels are 5, 10, 20, 50, 100, 200, 250, and 300 ppb for 446 abundances and 0.1, 1, 2, 5, 10, 20, 50, and 100‰ for the delta values.

2000; *Miller and Yung*, 2000]. Modeled distillation enrichment factors were calculated by a least-squares fit to equation (6) using simulated abundances restricted to the months, latitudes, and range of N_2O values coinciding with the measurements. The ZPE2 and HP models were each run using the GISS II meteorology.

[21] Overall, both photolysis models are found to be in good agreement (<20% difference) with the aircraft and balloon air-sampling measurements, showing slightly better agreement for the HP model (546 not withstanding). Larger discrepancies are observed with the enrichment factors from the recently re-analyzed solar occultation data (D. W. T. Griffith, personal communication, 2002). Here we compare separately with the weighted means of the mid-latitude and high latitude occultation enrichment factors. This latest analysis represents an improvement over the original (see D. W. T. Griffith et al. (Vertical profiles of isotopic fractionation of stratospheric N_2O, manuscript in preparation, 2003) for a detailed account) in that regions were selected that minimize systematic errors between isotopic analogues and improved line parameters for interfering gases were used. Also, one additional flight, in the Arctic winter vortex in January 2000, is now included. The occultation-to-occultation variation in enrichment factors was often considerable, even for balloon launches on consecutive days. While these enrichment factors are roughly 10‰ smaller than those originally reported by *Griffith et al.* [2000], they possess large uncertainties (up to 10‰) and their overall mean is still roughly 5–25‰ larger than the corresponding model values. The reason for the remaining systematic differences is unclear. Nonetheless, with 448 as the exception, the high latitude to mid-latitude ratios of enrichment factors are in reasonable agreement with both the ZPE2 and HP models.

[22] Model enrichment factors are observed to increase when the fit to equation (6) uses smaller N_2O abundances (i.e., generally higher altitudes). This feature has been identified in the balloon data by *Toyoda et al.* [2001] and *Röck-*

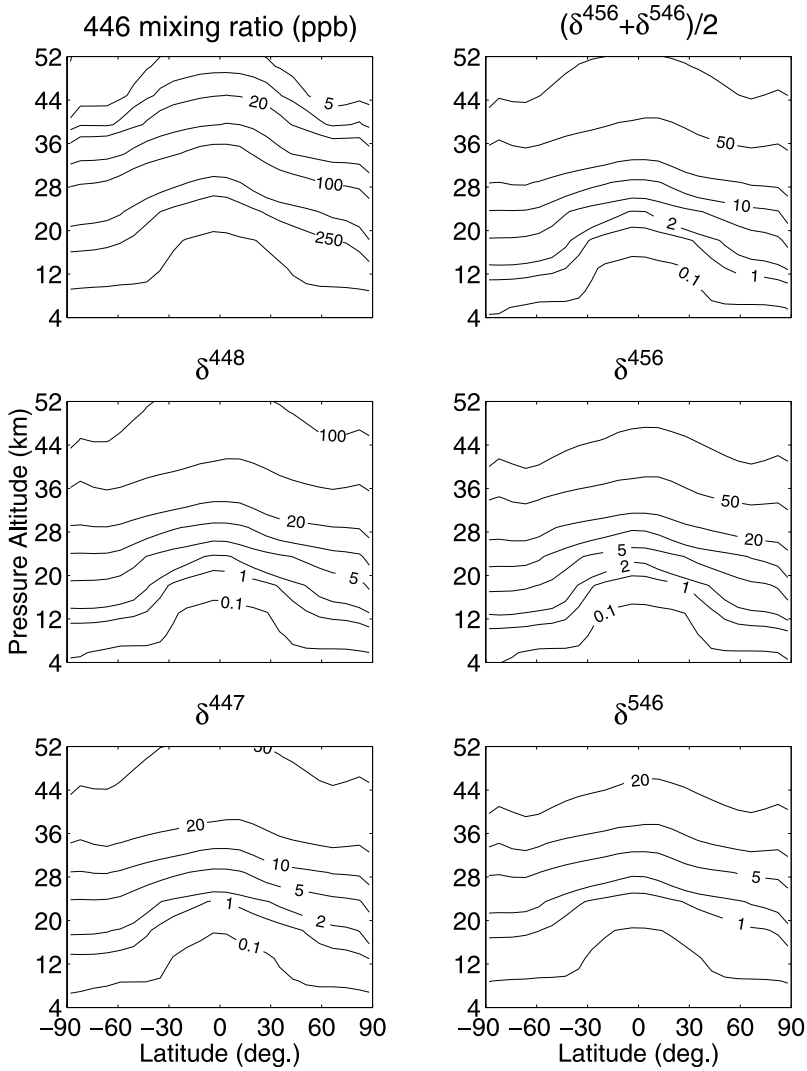

Figure 4. Zonal, annual mean HP N_2O abundance (in ppb) and delta values of 456, 546, 448, 447, and (456 + 546)/2 (in ‰). An effective lower boundary condition of $\delta = 0$ was used so these represent the shift in δ from the bulk troposphere. The ^{15}N panel is calculated as the mean of the HP 456 enrichment factors and the HP 456 enrichment factor scaled by 0.57 (see text). Contour levels are 5, 10, 20, 50, 100, 200, 250, and 300 ppb for 446 abundances and 0.1, 1, 2, 5, 10, 20, 50, and 100‰ for the delta values.

mann et al. [2001b]. When separate enrichment factors are calculated for two abundance regimes, larger values are found for the smaller N_2O abundances. Figure 5 further examines this, using 448 as an example, by plotting ϵ^{448} as a function of $-\ln f$. There is a curvature to the model data. The different slopes for 170–310 ppb and 10–170 ppb are shown (as dotted and dashed lines, respectively) to highlight this. A J-value e-fold curve based on the ratio 448 to 446 mean photolysis rates (which were derived from lifetimes) is also shown - it remains linear indicating it is transport which causes the departure from a simple Rayleigh distillation process. Thus observed stratospheric enrichment factors underpredict the true process-level photochemical enrichment factors, unless the effect of diffusion and mixing are taken into account (compare Table 1). In parallel with the recent findings on the net flux of odd-nitrogen from the stratosphere [*Olsen et al.*, 2001], an accurate approximation (to within 0.5‰) to the stratospheric distillation is obtained using mid-latitude measurements restricted to mixing ratios greater than 250 ppb.

4. Budget for N_2O Isotopic Analogues

[23] This budget comprises the flux-weighted isotopic composition of the N_2O sources and sinks. These budget terms for each isotopically rare species, in units of ‰ Tg(N) yr^{-1}, can be used to balance the budget, infer a trend, and identify the key components driving the trend. In constructing the budget, the delta value relative to that of the bulk troposphere is used. Thus, a source or sink with the same delta value as the troposphere has a zero term in the budget. The present-day 448 and (456 + 546)/2 budgets are presented in Table 3a for the ZPE2 model and Table 3b for a modified HP model. Individual assessments of the 456 and 546 budgets are not possible at this time due to a lack of information on ^{15}N site-preferences; however, recent meas-

Table 1. Stratospheric Budgets of N_2O Isotopic Analogues and Net Flux Enrichment Factors ϵL^X

	N_2O Isotopic Analogue				
	446 (Primary)	456	546	448	447
Burden, Tg	1490	–	–	–	–
Stratospheric loss, Tg(N)/yr	13.1	–	–	–	–
ZPE2 Model					
Lifetime, yr	113.8	115.8	115.0	115.2	114.6
Enrichment factor, ϵL^X, ‰	–	−17.0	−9.9	−11.9	−6.5
$\epsilon L^X/\epsilon L^{448}$	–	1.43	0.82	–	0.54
Enrichment factor, ϵL^X, ‰[a]	–	−14.2	−8.2	−10.0	−5.4
HP Model					
Lifetime, yr	113.8	116.0	114.3	115.4	114.6
Enrichment factor, ϵL^X, ‰	–	−19.1	−4.0[b]	−13.9	−7.3
$\epsilon L^X/\epsilon L^{448}$	–	1.38	0.28	–	0.52

[a]All model results are based on the GISS II 23 layer winds at 7.8° × 10° horizontal resolution, except for this row, which uses GISS II′ 31 layer winds at 8° × 10°, giving a lifetime for 446 of 161 yr.

[b]Given the known errors in the 546 cross sections, a modified HP model enrichment is calculated by scaling the 456 enrichment by the observed ratio in the lower stratosphere (0.57), giving −10.9‰.

urement techniques are able to distinguish them [e.g., *Pérez et al.*, 2001].

[24] As the HP model fractionation factor for 546 is known to be too small, a modified HP stratospheric enrichment factor for (456 + 546)/2 of −15.0‰ is based on a modified 546 enrichment (−10.9‰) that is scaled from the HP 456 enrichment by the measured 546:456 ratio of 0.57, a fairly robust quantity [*Yoshida and Toyoda*, 2000], see Table 1 footnote. Detailed source information is omitted from Table 3b as it is identical to that in Table 3a.

[25] The annual stratospheric sink strengths and enrichment factors are taken from the CTM simulations (see Table 1). The stratosphere is treated as a negative source of N_2O so the imbalance represents the sum of sources and sinks. Uncertainties are estimated at ±20%, based on a 17% uncertainty due to CTM deficiencies (i.e., 17% is the difference between the GISS II and II′ enrichment factors) and a 10% uncertainty from possible cross-section errors. Source categories and fluxes are taken from IPCC Chapter 4 [*Prather and Ehhalt*, 2001] but decreased slightly so that the net increase is 4.2 Tg(N)/yr, or 0.28%/yr, in general agreement with current estimates [*Prinn and Zander*, 1999]. Enrichment factors for individual sources are taken from the literature (see

Table 2. ZPE2 and HP Model Stratospheric Distillation Enrichment Factors Compared Measured Values[a]

			Enrichment Factors, ‰			
	Source	Range in N_2O, ppb	456	546	(456 + 546)/2	448
1	WB-57 aircraft[b]	180–310	–	–	−14.5	−12.9
	CTM (ZPE2)		−17.7	−10.2	−13.9	−12.4
	CTM (HP)		−19.9	−4.1	−12.0	−14.4
2a	Balloon occultation[c]	50–220	−55.5	−27.2	−41.3	−51.4
	CTM (ZPE2)		−28.7	−16.6	−22.6	−20.1
	CTM (HP)		−30.8	−6.7	−18.9	−23.0
2b	Balloon occultation[d]	5–270	−43.8	−18.3	−32.7	−22.3
	CTM (ZPE2)		−24.0	−13.9	−19.0	−16.9
	CTM (HP)		−25.3	−5.5	−15.6	−18.9
3	Balloon sample[e]	160–310	−24.5	−13.9	−19.2	−17.0
	CTM (ZPE2)		−19.1	−11.0	−15.1	−13.4
	CTM (HP)		−21.7	−4.4	−13.1	−15.7
4a	Balloon sample[f]	170–310	−22.9	−8.8	−15.9	−11.5
	CTM (ZPE2)		−17.3	−9.9	−13.6	−12.1
	CTM (HP)		−19.5	−4.0	−11.7	−14.1
4b	Balloon sample[f]	10–170	−40.9	−15.5	−28.6	−24.6
	CTM (ZPE2)		−29.8	−16.8	−23.3	−20.6
	CTM (HP)		−30.9	−6.6	−18.8	−23.0
5a	Balloon sample[g]	200–310	−21.3	−12.9	−17.1	−14.0
	CTM (ZPE2)		−18.3	−10.5	−14.4	−12.8
	CTM (HP)		−20.6	−4.2	−12.4	−15.0
5b	Balloon sample[g]	6–310	−33.4	−16.3	−24.9	−21.4
	CTM (ZPE2)		−25.7	−15.1	−20.9	−18.5
	CTM (HP)		−28.4	−6.0	−17.2	−20.1
Average model-measurement percent differences[h]						
	CTM (ZPE2)		−20.5	−5.3		−8.9
	CTM (HP)		−11.7	−63.8		+4.9

[a]For both model and measurements, the enrichment factor is calculated from an ensemble of points as the slope of the distribution with respect to the natural log of the 446 fraction. In the case of a Rayleigh distillation process (not the case for the stratosphere!), this enrichment factor is just the ratio of the mean lifetime of X to that of 446.

[b]33–68°N, January–March; *Rahn and Wahlen* [1997].

[c]34°N, April–September, mid-latitude occultations; values are statistically weighted means of 7 occultations with resultant standard errors of 7–10‰; *Griffith et al.* [2000] and D. W. T. Griffith (personal communication, 2002).

[d]64–68°N, high latitude occultations; values are statistically weighted means of 4 occultations with resultant standard errors of 4–6‰; *Griffith et al.* [2000] and D. W. T. Griffith (personal communication, 2002).

[e]40°N, September; derived from *Yoshida and Toyoda* [2000].

[f]39°N, May; *Toyoda et al.* [2001].

[g]Multiple launches; 18–69°N; *Röckmann et al.* [2001b].

[h](mod.-meas.)/meas. × 100%. Excludes comparison 2 (Balloon occultation).

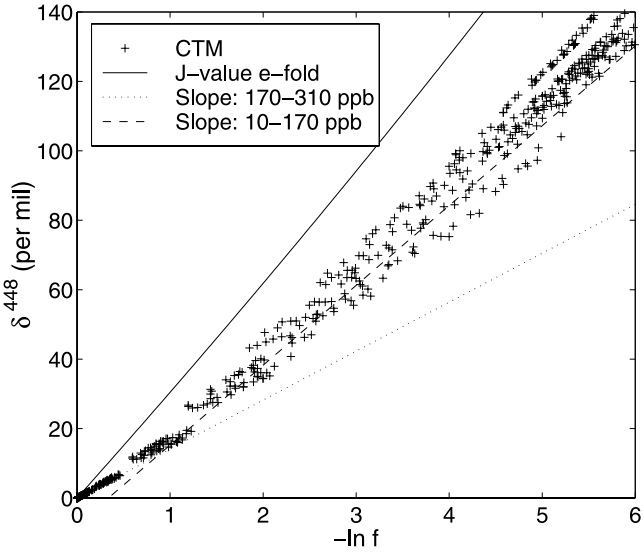

Figure 5. Delta values (using the HP model) for 448 as a function of $-\ln f$. Shown are CTM data points (+), best fit lines for 170–310 ppb (dotted) and 10–170 ppb (dashed), and the J-value e-fold curve (solid).

Table 3a) whenever possible. For some of the smaller source components, values are not available and so assumed values are used. Only uncertainties associated with the enrichment factors, not the source strength, are propagated here. These uncertainties are assumed to be at the 2/3-likelihood confidence interval and are combined as the square root of the summed squares.

[26] From Table 3a, the (456 + 546)/2 flux-weighted enrichment factors (FWEF) from sources is −262‰ Tg(N)/yr, which in steady-state with a nonfractionating sink would produce a delta value of −15.1‰ relative to the current mean troposphere. The ZPE2 model has a stratospheric sink that results in a net FWEF of +177‰ Tg(N)/yr, which in steady-state with a nonfractionated source would produce a delta value of +13.5‰. The imbalance of these two terms, −85‰ Tg(N)/yr, divided by the total mass of atmospheric N_2O implies a tropospheric trend in (456 + 546)/2 isotopic composition of −0.06 ± 0.06 ‰/yr. The modified HP model gives a larger stratospheric FWEF of +198‰ Tg(N)/yr and hence a small predicted trend of −0.04 ± 0.06 ‰/yr. The 448 FWEF from sources is −192‰ Tg(N)/yr, which in steady-state with a nonfractionated sink would produce a delta value of −11.1‰ relative to the current mean troposphere. The ZPE2 model has a stratospheric sink that results in a net FWEF of +156‰ Tg(N)/yr, which in steady-state with a nonfractionated source would produce a delta value of +11.9‰. The imbalance of these two terms, −36‰ Tg(N)/yr, is much smaller than that for (456 + 546)/2, and implies a tropospheric trend in 448 isotopic composition of −0.02 ± 0.10 ‰/yr. The HP model gives a larger stratospheric FWEF of +192‰ Tg(N)/yr and hence a small predicted trend of −0.01 ± 0.10 ‰/yr. For both isotopic analogues the agriculture and soil components are the two largest source terms, and by themselves, are sufficient to force a negative trend. A trend of −0.05 ‰/yr, while significant, would require several years of measurements to confirm given the 0.2‰ uncertainty level of current measurement techniques [e.g., *Rahn and Wahlen*, 2000; *Pérez et al.*, 2001]. However, analysis of firn air samples should be able to confirm this prediction. The trend uncertainties are clearly very large. Indeed, to within the quoted 2/3-likelihood confidence interval, the trends are not different from zero, and the inclusion of the flux uncertainties would make the overall uncertainties in the implied trends much larger still. The magnitude and enrichment of the source and sink budget

Table 3a. Budget for N_2O Isotopologues Based on the ZPE2 Model[a]

Budget Terms (Source/Sink)	446 Flux, Tg(N)/yr	(456 + 546)/2		448	
		‰	‰ Tg(N)/yr	‰	‰ Tg(N)/yr
Natural Sources					
Soil	5.9	−12 ± 10[b]	−71 ± 59	−16 ± 8[b]	−94 ± 47
Ocean	2.9	−1 ± 4[c]	−3 ± 12	−2 ± 8[c]	−6 ± 23
NH_3 oxidation	0.6	0 ± 10[d]	0 ± 6	10 ± 10[e]	6 ± 6
Anthropogenic Sources					
Agriculture	4.1	−43 ± 10[f]	−176 ± 41	−20 ± 4[f]	−82 ± 16
Industrial	1.3	0 ± 5[g]	0 ± 7	0 ± 5[g]	0 ± 7
Biomass burning	0.5	0 ± 5[d]	0 ± 3	0 ± 5[d]	0 ± 3
Cattle and feedlots	2.0	−6 ± 5[h]	−12 ± 10	−8 ± 5[h]	−16 ± 10
Total sources	17.3	(−15.1)	−262 ± 74	(−11.1)	−192 ± 56
Stratosphere	−13.1	−13.5 ± 2.7	+177 ± 35	−11.9 ± 2.4	+156 ± 31
Imbalance	4.2		−85 ± 82		−36 ± 64
Implied trend, ‰/yr			−0.06 ± 0.06		−0.02 ± 0.04
Measured trend,[i] ‰/yr			−0.041		−0.025

[a]Source strengths from IPCC 2001 adjusted slightly to give 4.2 Tg(N)/yr imbalance. The implied trend is the imbalance divided by the atmospheric N_2O burden, 1490 Tg(N). All delta values are relative to the mean tropospheric N_2O. Uncertainties in composition for individual sources are estimated based on cited references and *Rahn and Wahlen* [2000], and for the stratospheric sink they are set at 20% (see text). No uncertainty in the source strengths is assumed. All uncertainties are at the 2/3-likelihood confidence interval and are combined as the square root of the summed squares.
[b]Biased towards oxisoils, *Pérez et al.* [2000].
[c]*Kim and Craig* [1990].
[d]Assumed.
[e]*Röckmann et al.* [2001a].
[f]*Pérez et al.* [2001].
[g]*Rigby and Bates* [1986].
[h]Assumed to be between troposphere and soils.
[i]*Röckmann et al.* [2003], present-day trends as measured from Antarctic firn air samples; (456 + 546)/2 is mean of individual 456 and 546 values.

Table 3b. Budget for N_2O Isotopologues Based on the Modified HP Model[a]

Budget Terms (Source/Sink)	446 Flux, Tg(N)/yr	456 + 546)/2		448	
		‰	‰ Tg(N)/yr	‰	‰ Tg(N)/yr
Total Sources	17.3	(−15.1)	−262 ± 74	(−11.1)	−192 ± 56
Stratosphere	−13.1	−15.0 ± 3.0	+196 ± 39	−13.9 ± 2.8	+182 ± 37
Imbalance	4.2		−66 ± 84		−10 ± 68
Implied trend, ‰/yr			−0.04 ± 0.06		−0.01 ± 0.05
Measured trend, ‰/yr			−0.041		−0.025

[a]Source information as in Table 3a. See text, Table 1 for modified HP.

terms as well as the inferred trends are consistent within the derived uncertainty with our current knowledge and suggests that no new or exotic sources or processes need to be invoked to explain the observed tropospheric and stratospheric isotope distributions.

[27] As a further test of consistency of these budgets, we investigate how the tropospheric composition may have shifted since pre-industrial times. We use a one-box model of the atmosphere similar to that of *Rahn and Wahlen* [2000] but based on more recent source data and our model-derived stratospheric enrichment factors. The time series of *Kroeze et al.* [1999] is adopted for the various sources with all values scaled slightly so that present-day totals of natural and anthropogenic source strengths match those in Table 3a. For example, all natural sources were scaled by the factor of 9.4/9.6, where 9.6 Tg(N)/yr is the *Kroeze et al.* [1999] value and 9.4 Tg(N)/yr is from Table 3a. This model gives a pre-industrial total source which is consistent with a steady-state tropospheric abundance of 275 ppb. Using the modified HP model, the predicted shift between 1700 and 2000 is −4.7‰ for (456 + 546)/2 and −2.8‰ for 448. The shift in (456 + 546)/2 is reduced to −1.8‰ when the natural soil enrichment factor is used in the place of the agricultural soil enrichment factor which further highlights the importance of this quantity on the trends. This reduced value is consistent with *Rahn and Wahlen* [2000] who also used a natural soil enrichment factor for agricultural soils. The use of the natural soil enrichment factor has a much smaller impact on the shift in 448 - it is reduced but only to −2.5‰.

[28] These predictions can be compared with present-day trends obtained from Antarctic firn air samples [*Röckmann et al.*, 2003] in which the heavy isotope content of atmospheric N_2O was found to be decreasing at rates of about −0.041 ‰/yr for (456 + 546)/2 (based on the individual values reported for 456 and 546) and −0.025 ‰/yr for 448 (see Tables 3a and 3b). These are in rough agreement with the budget imbalances, although the ZPE2 model predicts too large a trend for (456 + 546)/2 and the modified HP model predicts too small a trend for 448. The *Röckmann et al.* [2003] total decrease since preindustrial times is estimated to be about −2‰ for (456 + 546)/2 and −1.2‰ for 448. Again, these numbers are in reasonable agreement with the one-box model predictions but only when the natural soil enrichment factor is used instead of the agricultural value.

5. The ^{17}O–^{18}O Mass Independent Anomaly

5.1. CTM Simulations

[29] It is generally believed that the majority of physical and chemical processes fractionate isotopes according to mass and these are termed 'mass-dependent'. Considering the 446, 447 and 448 isotopologues, a process is mass-dependent if (and only if) $\delta^{*447}/\delta^{*448} = 0.515$, where 0.515 is the mass-dependent coefficient determined experimentally from a range of commercial N_2O gases [*Cliff and Thiemens*, 1997]. Any departure from this relationship is referred to as 'mass-independent' and is quantified in terms of the mass-independent anomaly ($\Delta^{17}O$ in ‰):

$$\Delta^{17}O = \frac{R^{17}}{R_0^{17}} - \left(\frac{R^{18}}{R_0^{18}}\right)^{0.515} \approx \delta^{17}O - 0.515\left(\delta^{18}O\right)$$

$$= \delta^{*447} - 0.515\,\delta^{*448} \tag{7}$$

where the approximation arises from a small argument expansion.

[30] Measurements of δ^{447} and δ^{448} in the troposphere and lower stratosphere reveal mass-independent anomalies of 0.7 to 1.2‰, with the lower stratosphere values slightly larger [*Cliff and Thiemens*, 1997; *Cliff et al.*, 1999; *Röckmann et al.*, 2001a]. The origin of this mass-independent isotopic composition is uncertain although most researchers discount photolysis as the available mechanisms [*Johnson et al.*, 2001; *Yung and Miller*, 1997] use mass alone as an input variable in calculating photolytic fractionation factors. It may therefore be thought that the mass-independent anomaly has a chemical source. Nonetheless, the CTM ZPE2 simulation produced 447/448 ratios of 0.54 for the ZPE2 simulation and 0.52 for the HP simulation. Note that any increase over 0.515 of this ratio must arise from photolysis as loss through a reaction with $O(^1D)$ was made mass-dependent. In the ZPE2 simulation the 0.54 ratio can be traced back to the 447/448 ratio of wavelength shifts [*Miller and Yung*, 2000], i.e.,

$$\frac{\epsilon L^{447}}{\epsilon L^{448}} = \frac{\epsilon J^{447}}{\epsilon J^{448}} = \frac{\epsilon\sigma^{447}}{\epsilon\sigma^{448}} = \frac{\Delta\lambda^{447}}{\Delta\lambda^{448}} \tag{8}$$

where ϵJ^X is the enrichment in photolysis rate for species X, $\epsilon\sigma^X$ is the photolytic enrichment factor, and $\Delta\lambda^X$ is the ZPE2 wavelength shift. (The first equality in equation (8) is only approximate as photolysis represents only 90% of the loss.) From *Yung and Miller* [1997], $\Delta\lambda^{447}/\Delta\lambda^{448} = 0.545$ at 205 nm. Note that this ratio was not affected when the ZPE wavelength shift was doubled.

[31] The mass-dependent coefficient of 0.515 was determined experimentally and has some small uncertainty associated with it. Additionally, different processes will give slightly differing values due to differences in the mechanism of the mass dependence [*Assonov and Brenninkmeijer*, 2001]. For example, is the dependence linear in

mass, or vary as the square-root, and is it the mass of the entire molecule that is important, or simply the heavy isotope? This raises a further question of how close a ratio must be to 0.515 for a process to be considered mass-dependent. In the most literal sense both the ZPE2 and HP models exhibit some degree of mass-independence as they both depart from the expected 0.515 ratio. A future requirement of researchers in this field is to better define the tolerance of mass-dependence and perhaps identify in what way(s) a mass-dependent process depend(s) on mass. For the remainder of the study we avoid this issue and do not refer to the ZPE2 and HP models as either mass-independent or mass-dependent although we acknowledge that each predicts a nonzero mass-independent anomaly as defined in equation (7).

[32] The behaviors of the ZPE2 and HP mass-independent anomalies as a function of ln *f* are presented in Figure 6. Also shown are results from an additional CTM simulation in which 447 J-values were recalculated so that $\epsilon J^{447} = 0.515$ (ϵJ^{448}). For each case, an e-fold curve is shown representing Rayleigh distillation (i.e., the absence of transport),

$$\Delta^{17}O = \exp\left[\left(\epsilon J^{447}\right)t\right] - \exp\left[0.515\left(\epsilon J^{448}\right)t\right] \qquad (9)$$

where t is an effective time. The CTM values are generally smaller than their e-fold curves as the effect of transport is to mix $\delta^X = 0$ air from the mesosphere and upper stratosphere.

[33] For the $\epsilon J^{447} = 0.515$ (ϵJ^{448}) case, the J-value e-fold gives an identically zero mass-independent anomaly. The corresponding CTM run also predicts a zero anomaly (except for the uppermost stratosphere where the number of significant digits in the output file becomes a limiting factor). For the ZPE2 and HP cases, positive anomalies are found that increase linearly through the lower to mid-stratosphere and above this the increase becomes exponential. Measured anomalies from the laboratory experiments of *Röckmann et al.* [2001a] are also plotted on Figure 6. As these represent pure photolysis, they should be compared to the e-fold curves (as opposed to the CTM results). All anomalies in Figure 6 are calculated using the same mass-dependent coefficient (0.515) so it is fair to compare them even if another value is more appropriate for photolysis. The measurements hover near zero are so are most consistent with the $\epsilon J^{447} = 0.515(\epsilon J^{448})$ J-values, but are also in reasonable agreement with the HP model. Conclusions regarding the ability of the HP model to predict the size of the anomaly will require measurements to greater e-folds.

5.2. A Simple Model of Mass-Independent Anomalies

[34] Previous studies have invoked additional mass-independent sources or processes to help explain the observed mass-independent anomaly [e.g., *Cliff and Thiemens*, 1997; *Röckmann et al.*, 2001a]. We examine several source scenarios using a one-dimensional vertical diffusion model with globally, annually averaged loss frequencies [*Prather*, 1998]. When loss frequencies in the 1-D model are adjusted so that its stratospheric enrichment factors match that of the GISS-II CTM, the δ* values and mass-independent anomalies likewise match the CTM, and the lifetime of 446 is 113.8 years. Note that for this simple model source fluxes are used with an isotopic composition as given in Table 3a and so we now consider δ instead of δ*.

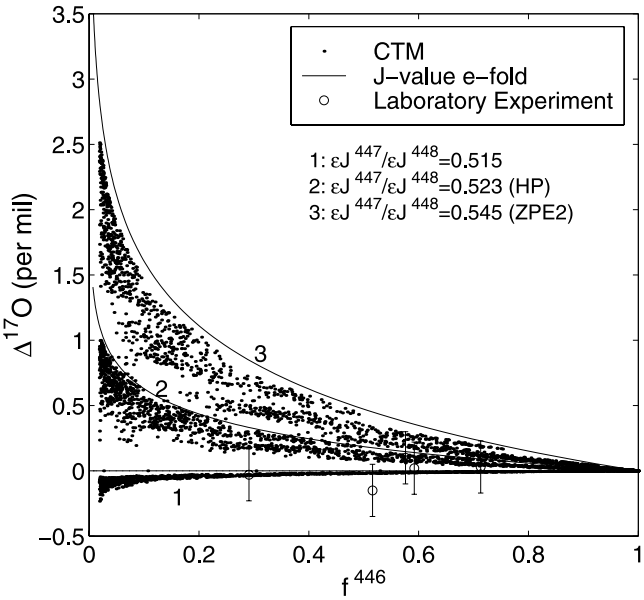

Figure 6. CTM mass-independent anomalies, $\Delta^{17}O$, as a function of the 446 abundance relative to 310 ppb. Three different photolysis models are used: (1) the scaled zero-point energy (ZPE2) shift model [*Yung and Miller*, 1997], (2) the time-dependent Hermite propagator model (HP) [*Johnson et al.*, 2001], and (3) $\epsilon J^{447} = 0.515$ (ϵJ^{448}) J-values. Also shown for each is a corresponding J-value e-fold line which represents the expected $\Delta^{17}O$ for a pure chemical loss (without transport, see text). The $\epsilon J^{447} = 0.515$ (ϵJ^{448}) e-fold is identically zero. Experimental data points are from *Röckmann et al.* [2001a].

[35] Five source scenarios were modeled and the resulting values of $\Delta^{17}O$ from the troposphere or lowermost stratosphere (effectively the same) are tabulated in Table 4. Each source scenario was run twice: initially using the $\epsilon J^{447} = 0.515$ (ϵJ^{448}) J-values and repeated using the ZPE2 J-values. For each scenario, results from the HP model lie roughly midway between the other two and so are not explicitly considered. A three-isotope plot (δ^{447} vs. δ^{448}), Figure 7, was created showing a subset of these results. In this type of plot the mass-independent anomaly is measured by the vertical distance from the data point to the mass-dependent fractionation line. The range of δ^{448} on this plot corresponds to the troposphere and lower stratosphere. For comparison, the measurements of mass-independent anomalies from *Cliff and Thiemens* [1997], *Cliff et al.* [1999] and *Röckmann et al.* [2000] are also plotted. Source scenario 1 includes only standard mass-dependent sources (i.e., those in Table 3a). The $\epsilon J^{447} = 0.515$ (ϵJ^{448}) J-values produced a zero anomaly while the ZPE2 J-values gave an anomaly of about 0.3‰, roughly one third to one half of that measured.

[36] Over the years a number of stratospheric sources of N_2O have been hypothesized [e.g., *Zellner et al.*, 1992; *McElroy and Jones*, 1996; *Zipf and Prasad*, 1998]. For source scenario 2 we examine the Zellner et al. reaction sequence:

$$NO_2 + h\nu \longrightarrow NO_2^* \qquad (10a)$$

$$NO_2^* + N_2 \longrightarrow N_2O + NO \qquad (10b)$$

Table 4. Mass-Independent Anomalies ($\Delta^{17}O$) for Optional N_2O Source Scenarios[a]

Source Scenario	$\Delta^{17}O$ (‰) for 447–448 Photolysis	
	ZPE2	$\epsilon J^{447} = 0.515\ (\epsilon J^{448})$
1 Standard mass-dependent sources	0.3	0.0
2 Hypothetical middle stratosphere source of 0.4 Tg(N)/yr at $\delta^{447} = \delta^{448} = 100‰$: $NO_2^* + N2 \rightarrow N_2O + NO$[b]	1.1	0.8
3 Known tropospheric source of 0.6 Tg/yr fractionated at $\delta^{447} = \delta^{448} = 40‰$: $NH_2 + NO_2 \rightarrow N_2O + H_2O$	1.4	1.2
4 Hypothetical tropospheric & stratosphere source of 0.2 Tg(N)/yr at $\delta^{447} = \delta^{448} = 100‰$: $O(^1D) + N_2 + M \rightarrow N_2O + M$[c]	1.2	1.0
5 Known stratospheric source of 0.025 Tg(N)/yr fractionated at $\delta^{447} = \delta^{448} = 100‰$: $N + NO_2 \rightarrow N_2O + O$	0.4	0.1

[a]Isotopic compositions represent the bulk (i.e., troposphere and lowermost stratosphere). Standard sources in all cases are mass-dependent. Calculations taken from 1-D vertical diffusion model fitted to CTM ZPE2.
[b]*Zellner et al.* [1992].
[c]*Estupiñán et al.* [2002].

A source strength of 0.4 Tg(N)/yr between 26 and 38 km altitude with an isotopic composition of $\delta^{447} = \delta^{448} = 100‰$ is adopted. The size of this source is feasible in light of results from another study that placed an upper limit of 5.3 Tg(N)/yr on the N_2O yield from this sequence [*Olsen et al.*, 2001]. Moreover, a 0.4 Tg(N)/yr source is also easily within the constraints imposed by observed N_2O - NO_y correlations in the stratosphere [*Nevison et al.*, 1999; *Olsen et al.*, 2001]. Recent mid-stratospheric ozone isotope measurements show a mass independent fractionation of roughly $\delta^{18}O = \delta^{17}O = 100‰$ [*Krankowsky et al.*, 2000; *Mauersberger et al.*, 2001]. Another oxidant, H_2O_2, is also observed to possess a mass-independent fractionation [*Savarino and Thiemens*, 1999]. Given the rapid exchange of O between ozone, reactive nitrogen, and reactive hydrogen in the stratosphere, it is very likely that NO_2 inherits at least some degree of this signature. Further, a recent modeling study by *Lyons* [2001] predicted a mid-stratospheric $\Delta^{17}O$ for NO and NO_2 of 70–80‰ which amounts to an isotopic composition of about 150‰ assuming $\delta^{18}O = \delta^{17}O$. Source scenario 2 predicted an anomaly of 0.8‰ for $\epsilon J^{447} = 0.515\ \epsilon J^{448}$ J-values and 1.1‰ for the ZPE2 J-values - both values fall within observations. As shown in Figure 7, source scenario 2 increases the tropospheric δ^{448} fractionation by about 1.5‰ although this still remains within the range reported in the literature.

[37] Source scenario 3 is one proposed by *Röckmann et al.* [2001a] in which oxidation of NH_3 is the source of mass-independence:

$$NH_3 + OH \longrightarrow NH_2 + H_2O \tag{11a}$$

$$NH_2 + NO_2 \longrightarrow N_2O + H_2O \tag{11b}$$

The IPCC 2001 source strength of 0.6 Tg(N)/yr is adopted with an isotopic composition of $\delta^{18}O = \delta^{17}O = 40‰$, (so that this source has a $\Delta^{17}O$ of 20‰). This choice of composition is based on similar arguments as for the anomalous distribution of oxygen nuclides in stratospheric NO_2, but is less than that predicted by the *Lyons* [2001] study. Source number 3 produced the largest anomalies: 1.4‰ for ZPE2 J-values and 1.2‰ for $\epsilon J^{447} = 0.515\ \epsilon J^{448}$ J-values. These anomalies are slightly larger than the observations and a 20–30% reduction in the source strength or delta value would give results which are the most consistent with the observations. As this source was already included in the 'standard sources' (but as a mass-dependent source) there was no change in δ^{448} values (see Figure 7) and so only 447 was affected.

[38] Source scenario 4 is one originally proposed by *Zipf and Prasad* [1998] and recently re-examined in the laboratory by *Estupiñán et al.* [2002]. It involves the formation of N_2O through the reaction:

$$O(^1D) + N_2 + M \longrightarrow N_2O + M \tag{12}$$

The source of $O(^1D)$ is the photolysis of ozone, so the N_2O inherits the mass-independence of ozone directly. *Estupiñán et al.* [2002] estimate a global source of about 0.2 Tg(N)/yr with a profile from the troposphere to mid-stratosphere, peaking near the surface and again at about 25 km. At $\delta^{448} = \delta^{447} = 100‰$. Source 4 predicts anomalies of 1.2 and 1.0‰ for the ZPE2 and $\epsilon J^{447} = 0.515\ \epsilon J^{448}$ J-values, respectively. With this magnitude and composition, source 4 alone could explain the observed anomaly.

[39] Source scenario 5 represents the small amount of stratospheric NO_y which is converted back to N_2O through the sequence:

$$NO + h\nu \longrightarrow N + O \tag{13a}$$

$$N + NO_2 \longrightarrow N_2O + O \tag{13b}$$

This source is small, about 0.025 Tg(N)/yr, and is accounted for in the CTM loss frequencies with a fractionation factor of zero. We again use $\delta^{448} = \delta^{447} = 100‰$. This source predicts anomalies of 0.4 and 0.1 for the ZPE2 and $\epsilon J^{447} = 0.515\ \epsilon J^{448}$ J-values, respectively. Thus source scenario 5 explains roughly 10% of the observed anomaly. Of the in situ source scenarios examined (numbers 2 through 5), all but the last are able to explain a large portion of the observed mass-independent anomaly. The altitude of these

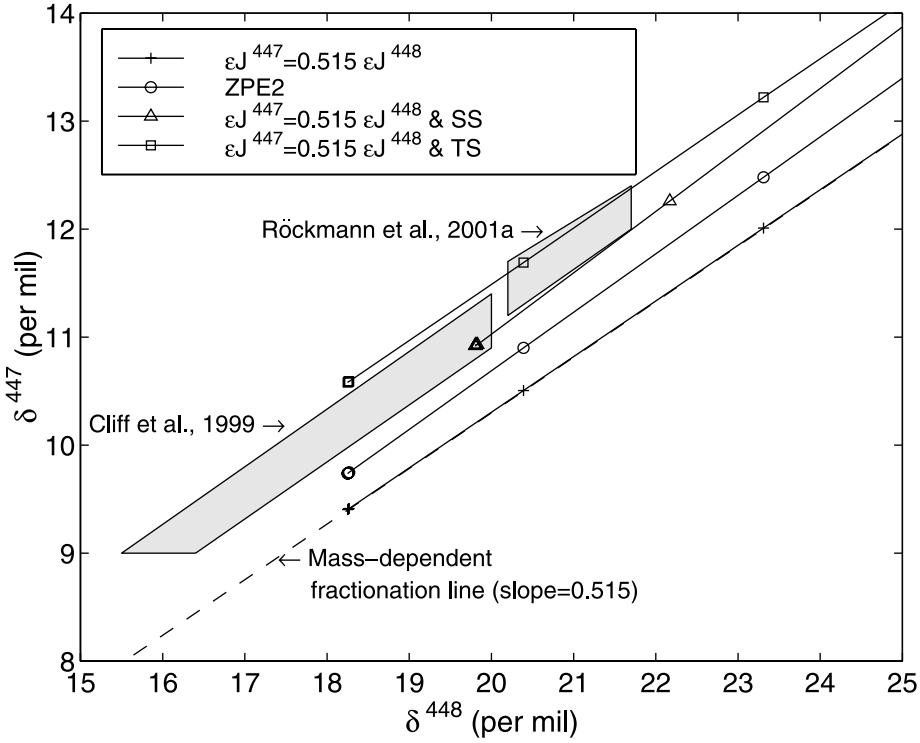

Figure 7. A three isotope plot (δ^{447} vs. δ^{448}) of 1-D vertical diffusion model results for four source scenarios (see Table 4): (1) no additional source and $\epsilon J^{447} = 0.515\ \epsilon J^{448}$ J-values, (2) no additional source and J-values from ZPE2 model [*Yung and Miller*, 1997], (3) as (1) but with an additional stratospheric source (SS) of 0.4 Tg(N)/yr and $\delta^{447} = \delta^{448} = 100‰$ injected at 26–38 km, and (4) as (1) but with 0.6 Tg(N)/yr of the standard tropospheric source (TS) fractionated at $\delta^{447} = \delta^{448} = 40‰$. Also shown (as shaded blocks) are tropospheric and lower stratospheric measurements of the mass-independent anomaly [*Cliff and Thiemens*, 1997; *Cliff et al.*, 1999; *Röckmann et al.*, 2001a]. In this plot, the mass-independent anomaly, $\Delta^{17}O$, is the vertical difference between the data point and the mass-dependent fractionation line.

in situ sources is an important factor in determining the size of the modeled anomaly. That is, the model predicts the anomaly is largest in the vicinity of the source. This is why sources 3 and 4 predict the largest anomalies despite the fact that they did not have the largest strengths or mass-independent compositions. Indeed, the location of the source determines to a large extent the profile of the anomaly, and thus a vertical sounding of the anomaly would be very useful in constraining the location of the source, even if it is only a small fraction the global source.

6. Summary and Conclusions

[40] A three-dimensional chemical transport model (CTM) was used to model the five most abundant isotopic analogues of N_2O: $^{14}N^{14}N^{16}O$ (446, the primary species), $^{14}N^{15}N^{16}O$ (456), $^{15}N^{14}N^{16}O$ (546), $^{14}N^{14}N^{18}O$ (448), and $^{14}N^{14}N^{17}O$ (447). Two different chemistry models for N_2O photolysis were used to described stratospheric enrichment. In order to agree with recent experimental results, the wavelength shift of the zero-point energy shift model (ZPE) was increased by a factor of 2 (ZPE2). The ZPE2 model predicted stratospheric enrichment factors in good agreement with measurements. The Hermite propagator (HP) model generally performed better than the ZPE2 model when compared with laboratory measurements and observations of stratospheric enrichment, and it did not require arbitrary scaling. The exception to this was 546, for which the HP cross-section enrichment is underestimated. This shortcoming is most likely connected to the use of a two-dimensional potential energy surface in the calculation. Work is underway by one author (MSJ) to resolve this error. As different measurements of the 546:456 ratio in the lower stratosphere appear to be consistent [e.g., *Yoshida and Toyoda*, 2000], it is possible to derive a 546 fractionation factor consistent with the HP model for the other isotopic analogues by scaling.

[41] Combining CTM-derived distributions from the stratospheric sink with current estimates of isotopic distributions within N_2O sources allows for the construction of a species-specific budget, of flux-weighted enrichment factor that appears to be out of balance. This analysis predicts a clear negative trend for the combined (456 + 546)/2 isotopomers of about -0.05 ± 0.06 ‰/yr. For the 448 isotopologue the predicted imbalance is much smaller, and the trend, -0.02 ± 0.05 ‰/yr, is much smaller than the uncertainty. Measurement of this trend may provide a key constraint on the anthropogenic sources of N_2O that cannot be derived from direct budgetary analysis. The CTM also predicts that the oxygen nuclides in $^{14}N^{14}N^{17}O$ and

$^{14}N^{14}N^{18}O$ will be fractionated in a manner that produces a nonzero mass-independent anomaly which can be traced to the ZPE2 and HP models (assuming a mass-dependent coefficient of 0.515 is appropriate). These two models can reproduce at most half of the observed anomaly, and thus other mechanisms must be at least in part responsible for the observed 1‰ anomaly. Several feasible stratospheric and tropospheric source scenarios were examined with a simplified model and were substantial enough to explain some or all of the observed anomaly.

[42] This study indicates that the major advances in understanding anthropogenic control over nitrous oxide must focus on the major sources (agricultural and natural soils) and the current trends in the mixing ratios of isotopic analogues in the atmosphere.

[43] **Acknowledgments.** M.J.P. acknowledges the support of the atmospheric chemistry programs of NSF and NASA as well as the NASA Atmospheric Effects of Aviation Program. M.S.J. acknowledges the support of the Danish Natural Science Research Council and the Nordic Academy for Advanced Study. The authors wish to thank D. W. T. Griffith for sharing balloon occultation data prior to publication, T. Pérez for helpful discussions, and an anonymous reviewer for detailed and thoughtful comments.

References

Andrews, D. G., and M. E. McIntyre, Generalized Eliassen-Palm and Charney-Drazin theorems for waves on axisymmetric mean flows in compressible atmospheres, *J. Atmos. Sci.*, *35*, 175–185, 1978.

Assonov, S. S., and C. A. M. Brenninkmeijer, A new method to determine the ^{17}O isotopic abundance in CO_2 using isotope exchange with a solid oxide, *Rapid Commun. Mass Spectrom.*, *15*, 2426–2437, 2001.

Avallone, L. M., and M. J. Prather, Tracer-tracer correlations: Three-dimensional model simulations and comparisons to observations, *J. Geophys. Res.*, *102*, 19,233–19,246, 1997.

Bates, D. R., and P. B. Hays, Atmospheric nitrous oxide, *Planet. Space Sci.*, *15*, 189–198, 1967.

Battle, M., M. Bender, T. Sowers, P. P. Tans, J. H. Butler, J. W. Elkins, T. Conway, N. Zhang, P. Lang, and A. D. Clarke, Atmospheric gas concentrations over the past century measured in air from firn at South Pole, *Nature*, *383*, 231–235, 1996.

Brown, A., P. Jimeno, and G. G. Balint-Kurti, Photodissociation of N_2O, I, ab initio potential energy surfaces for the low-lying electronic states $1A'$, $2\ 1A'$, and $1\ 1A''$, *J. Phys. Chem. A*, *103*, 11,089–11,095, 1999.

Cliff, S. S., and M. H. Thiemens, The $^{18}O/^{16}O$ and $^{17}O/^{16}O$ ratios in atmospheric nitrous oxide: A mass-independent anomaly, *Science*, *278*, 1774–1776, 1997.

Cliff, S. S., C. A. M. Brenninkmeijer, and M. H. Thiemens, First measurement of the $^{18}O/^{16}O$ and $^{17}O/^{16}O$ ratios in stratospheric nitrous oxide: A mass-independent anomaly, *J. Geophys. Res.*, *104*, 16,171–16,175, 1999.

Crutzen, P. J., The influence of nitrogen oxides on the atmospheric ozone content, *Q. J. R. Meteorol. Soc.*, *96*, 320–325, 1970.

Dunkerton, T. J., On the mean meridional mass motions of the stratosphere and mesosphere, *J. Atmos. Sci.*, *35*, 2325–2333, 1978.

Estupiñán, E. G., J. M. Nicovich, J. Li, D. M. Cunnold, and P. H. Wine, An investigation of N_2O production from 266 nm and 532 nm laser flash photolysis of $O_3/N_2/O_2$ mixtures, *J. Phys. Chem. A*, *106*, 5880–5890, 2002.

Flückiger, J., A. Dällenbach, T. Blunier, B. Stauffer, T. F. Stocker, D. Raynaud, and J.-M. Barnola, Variations in atmospheric N_2O concentration during abrupt climatic changes, *Science*, *285*, 227–230, 1999.

Griffith, D. W. T., G. C. Toon, B. Sen, J. F. Balvier, and R. A. Toth, Vertical profiles of nitrous oxide isotopomer fractionation measured in the stratosphere, *Geophys. Res. Lett.*, *27*, 2485–2488, 2000.

Hall, T. M., and M. J. Prather, Seasonal evolution of N_2O, O_3, and CO_2: Three-dimensional simulations of stratospheric correlations, *J. Geophys. Res.*, *100*, 16,699–16,720, 1995.

Johnson, M. S., G. D. Billing, A. Gruodis, and H. M. Janssen, Photolysis of nitrous oxide isotopomers studied by time-dependent Hermite propagation, *J. Phys. Chem. A*, *105*, 8672–8680, 2001.

Johnston, J. C., S. C. Cliff, and M. H. Thiemens, Measurement of multioxygen isotopic ($\delta^{18}O$ and $\delta^{17}O$) fractionation factors in the stratospheric sink reactions of nitrous oxide, *J. Geophys. Res.*, *100*, 16,801–16,804, 1995.

Kim, K.-R., and H. Craig, Two-isotope characterization of N_2O in the Pacific Ocean and constraints on its origin in deep water, *Nature*, *347*, 58–61, 1990.

Koch, D., and D. Rind, $^{10}Be/^{7}Be$ as a tracer of stratospheric transport, *J. Geophys. Res.*, *103*, 3907–3917, 1998.

Krankowsky, D., P. Lämmerzahl, and K. Mauersberger, Isotopic measurements of stratospheric ozone, *Geophys. Res. Lett.*, *27*, 2593–2595, 2000.

Kroeze, C., A. Mosier, and L. Bouwman, Closing the global N_2O budget: A retrospective analysis 1500–1994, *Global Biogeochem. Cycles*, *13*, 1–8, 1999.

Lyons, J. R., Transfer of mass-independent fractionation in ozone to other oxygen-containing radicals in the atmosphere, *Geophys. Res. Lett.*, *28*, 3231–3234, 2001.

Mauersberger, K., P. Lämmerzahl, and D. Krankowsky, Stratospheric ozone isotope enrichments: Revisited, *Geophys. Res. Lett.*, *28*, 3155–3158, 2001.

McElroy, M. B., and D. B. A. Jones, Evidence for an additional source of atmospheric N_2O, *Global Biogeochem. Cycles*, *10*, 651–659, 1996.

McElroy, M. B., and J. C. McConnell, Nitrous oxide: Natural source of stratospheric NO, *J. Atmos. Sci.*, *28*, 1095–1103, 1971.

McLinden, C. A., S. Olsen, B. Hannegan, O. Wild, M. J. Prather, and J. Sundet, Stratospheric ozone in 3-D models: A simple chemistry and the cross-tropopause flux, *J. Geophys. Res.*, *105*, 14,653–14,665, 2000.

Miller, C. E., and Y. L. Yung, Photo-induced isotopic fractionation, *J. Geophys. Res.*, *105*, 29,039–29,051, 2000.

Mosier, A. R., J. M. Duxbury, J. R. Freney, O. Heinemeyer, K. Minami, and D. E. Johnson, Mitigating agricultural emissions of methane, *Clim. Change*, *40*, 39–80, 1998.

Nevison, C. D., E. R. Keim, S. Solomon, D. W. Fahey, J. W. Elkins, M. Loewenstein, and J. R. Podolske, Constraints on N_2O sinks inferred from observed tracer correlations in the lower stratosphere, *Global Biogeochem. Cycles*, *13*, 737–742, 1999.

Olivier, J. G. J., A. F. Bouwman, K. W. van der Hoek, and J. J. M. Berdowski, Global air emission inventories for anthropogenic sources of NO_x, NH_3 and N_2O in 1990, *Environ. Pollut.*, *102*, 135–148, 1998.

Olsen, S. C., C. A. McLinden, and M. J. Prather, The stratospheric N_2O-NO_y system: Testing uncertainties is a three-dimensional framework, *J. Geophys. Res.*, *106*, 28,771–28,784, 2001.

Park, J. H., M. K. W. Ko, C. H. Jackman, R. A. Plumb, J. A. Kaye, and K. H. Sage (Eds.), *Models and Measurements Intercomparison II, NASA Tech. Memo., NASA/TM-199-209554*, 502 pp., 1999.

Pérez, T., S. E. Trumbore, S. C. Tyler, E. A. Davidson, M. Keller, and P. B. de Camargo, Isotopic variability of N_2O emissions from tropical forest soils, *Global Biogeochem. Cycles*, *14*, 525–535, 2000.

Pérez, T., S. E. Trumbore, S. C. Tyler, P. A. Matson, I. Ortiz-Monasterio, T. Rahn, and D. W. T. Griffith, Identifying the agricultural imprint on the global N_2O budget using stable isotopes, *J. Geophys. Res.*, *106*, 9869–9878, 2001.

Prather, M. J., Time scales in atmospheric chemistry: Coupled perturbations to N_2O, NO_y, and O_3, *Science*, *279*, 1339–1341, 1998.

Prather, M., and D. Ehhalt, Atmospheric chemistry and greenhouse gases, in *Climate Change 2001: The Scientific Basis, Contribution of Working Group I to the Third Assessment Report of the Intergovernmental Panel on Climate Change*, edited by J. T. Houghton et al., pp. 239–287, Cambridge Univ. Press, New York, 2001.

Prinn, R. G., and R. Zander, Long-lived ozone-related compounds, in *Scientific Assessment of Ozone Depletion: 1998*, *Rep. 44*, pp. 1.1–1.54, World Meteorol. Organ. Global Ozone Res. Monit. Proj., Geneva, 1999.

Prinn, G., et al., A history of chemically and radiatively important gases in air deduced from ALE/GAGE/AGAGE, *J. Geophys. Res.*, *105*, 17,751–17,792, 2000.

Rahn, T., and M. Wahlen, Stable isotope enrichment in stratospheric nitrous oxide, *Science*, *278*, 1776–1778, 1997.

Rahn, T., and M. Wahlen, A reassessment of the global isotopic budget of atmospheric nitrous oxide, *Global Biogeochem. Cycles*, *14*, 537–543, 2000.

Rahn, T., H. Zhang, M. Wahlen, and G. A. Blake, Stable isotope fractionation during ultraviolet photolysis of N_2O, *Geophys. Res. Lett.*, *25*, 4489–4492, 1998.

Ramanathan, V., R. J. Cicerone, H. B. Singh, and J. T. Kiehl, Trace gas trends and their potential role in climate change, *J. Geophys. Res.*, *90*, 5547–5566, 1985.

Rigby, D., and B. D. Bates, The isotopic composition of nitrogen in Australian coals and oil shales, *Chem. Geol.*, *58*, 273–282, 1986.

Rind, D., R. Suozzo, N. K. Balachandran, A. Lacis, and G. Russell, The GISS global climate/middle atmosphere model, I, Model structure and climatology, *J. Atmos. Sci.*, *45*, 329–370, 1988.

Rind, D., J. Lerner, and C. McLinden, Changes of tracer distribution in the doubled CO_2 climate, *J. Geophys. Res.*, *106*, 28,061–28,079, 2001.

Röckmann, T., C. A. M. Brenninkmeijer, M. Wollenhaupt, J. N. Crowley, and P. J. Crutzen, Measurement of the isotopic fractionation of $^{15}N^{14}N^{16}O$, $^{14}N^{15}N^{16}O$ $^{14}N^{14}N^{18}O$ in the UV photolysis of nitrous oxide, *Geophys. Res. Lett.*, *27*, 1399–1402, 2000.

Röckmann, T., J. Kaiser, J. N. Crowley, C. A. M. Brenninkmeijer, and P. J. Crutzen, The origin of the anomalous or "mass-independent" oxygen isotope fractionation in tropospheric N_2O, *Geophys. Res. Lett.*, *28*, 503–506, 2001a.

Röckmann, T., J. Kaiser, C. A. M. Brenninkmeijer, J. N. Crowley, R. Borchers, W. A. Brand, and P. J. Crutzen, Isotopic enrichment of nitrous oxide ($^{15}N^{14}NO$, $^{14}N^{15}NO$, $^{14}N^{14}N^{18}O$) in the stratosphere and in the laboratory, *J. Geophys. Res.*, *106*, 10,403–10,410, 2001b.

Röckmann, T., J. Kaiser, and C. A. M. Brenninkmeijer, The isotopic fingerprint of the pre-industrial and the anthropogenic N_2O source, *Atmos. Chem. Phys.*, in press, 2003.

Sander, S. P., et al., Chemical kinetics and photochemical data for use in stratospheric modeling: Evaluation 13, *JPL Publ., 00-003*, 2000.

Savarino, J., and M. H. Thiemens, Analytical procedure to determine both ^{18}O and ^{17}O of H_2O_2 in natural water and first measurements, *Atmos. Environ.*, *33*, 3683–3690, 1999.

Toyoda, S., N. Yoshida, T. Urabe, S. Aoki, T. Nakazawa, S. Sugawara, and H. Honda, Fractionation of N_2O isotopomers in the stratosphere, *J. Geophys. Res.*, *106*, 7515–7522, 2001.

Turatti, F., D. W. T. Griffith, S. R. Wilson, M. B. Esler, T. Rahn, H. Zhang, and G. A. Blake, Positionally dependent ^{15}N fractionation factors in the UV photolysis of N_2O determined by high resolution FTIR spectroscopy, *Geophys. Res. Lett.*, *27*, 2489–2492, 2000.

Umemoto, H., $^{14}N/^{15}N$ isotope effect in the UV photodissociation of N_2O, *Chem. Phys. Lett.*, *314*, 267–272, 1999.

Weiss, R. F., The temporal and spatial distribution of tropospheric nitrous oxide, *J. Geophys. Res.*, *86*, 7185–7195, 1981.

Wild, O., and M. J. Prather, Excitation of the primary tropospheric chemical mode in a global three-dimensional model, *J. Geophys. Res.*, *105*, 24,647–24,660, 2000.

Yoshida, N., and S. Toyoda, Constraining the atmospheric N_2O budget from intramolecular site preference in N_2O isotopomers, *Nature*, *405*, 330–334, 2000.

Yung, Y. L., and C. E. Miller, Isotopic fractionation of stratospheric nitrous oxide, *Science*, *278*, 1778–1780, 1997.

Yung, Y. L., W. C. Wang, and A. A. Lacis, Greenhouse effects due to atmospheric nitrous oxide, *Geophys. Res. Lett.*, *3*, 619–621, 1976.

Zellner, R., D. Hartmann, and I. Rosner, N_2O formation in the reactive collisional quenching of NO_3^* and NO_2^* by N_2, *Ber. Bunsen-Gesellsch. Phys. Chem.*, *96*, 385–390, 1992.

Zhang, H., P. O. Wennberg, V. H. Wu, and G. A. Blake, Fractionation of $^{14}N^{15}N^{16}O$ and $^{15}N^{14}N^{16}O$ during photolysis at 213 nm, *Geophys. Res. Lett.*, *27*, 2481–2484, 2000.

Zipf, E. C., and S. S. Prasad, Experimental evidence that excited ozone is a source of nitrous oxide, *Geophys. Res. Lett.*, *25*, 4333–4336, 1998.

M. S. Johnson, Department of Chemistry, University of Copenhagen, Universitetsparken 5, DK-2100 Copenhagen Ø, Denmark. (msj@kiku.dk)

C. A. McLinden, Meteorological Service of Canada, 4905 Dufferin Street, Downsview, Ontario M3H 5T4, Canada. (chris.mclinden@ec.gc.ca)

M. J. Prather, Department of Earth System Science, University of California, Irvine, Irvine, CA 92697-3100, USA. (mprather@uci.edu)